

Attitude-Guided Loop Closure for Cameras with Negative Plane

Ze Wang^{1,4}, Kailun Yang², Peng Li¹, Fei Gao^{3,4} and Kaiwei Wang¹

Abstract—Loop closure is an important component of Simultaneous Localization and Mapping (SLAM) systems. Large Field-of-View (FoV) cameras have received extensive attention in the SLAM field as they can exploit more surrounding features on the panoramic image. In large-FoV VIO, for incorporating the informative cues located on the negative plane of the panoramic lens, image features are represented by a three-dimensional vector with a unit length. While the panoramic FoV is seemingly advantageous for loop closure, the benefits cannot easily be materialized under large-attitude-angle differences, where loop-closure frames can hardly be matched by existing methods. In this work, to fully unleash the potential of ultra-wide FoV, we propose to leverage the attitude information of a VIO system to guide the feature point detection of the loop closure. As loop closure on wide-FoV panoramic data further comes with a large number of outliers, traditional outlier rejection methods are not directly applicable. To tackle this issue, we propose a loop closure framework with a new outlier rejection method based on the unit length representation, to improve the accuracy of LF-VIO. On the public PALVIO dataset, a comprehensive set of experiments is carried out and the proposed LF-VIO-Loop outperforms state-of-the-art visual-inertial-odometry methods. Our code will be open-sourced at <https://github.com/flysoaryun/LF-VIO-Loop>.

I. INTRODUCTION

Pose estimation has attracted extensive attention in the field of robotics and autonomous driving [1]–[4]. It is often combined with omnidirectional cameras to exploit the large Field-of-View (FoV) of panoramic images [5], [6] for a more robust prediction with 360° surrounding features [7]–[9]. Yet, in many real-world application scenarios without the Global Navigation Satellite System (GNSS), Visual-Inertial-Odometry (VIO) and Visual Odometry (VO) tend to increase the cumulative error over time. When the drift is too large, it may cause a significant impact on the entire robotic system and the navigation task [10], [11].

Loop closure and pose graph optimization can help estimate and eliminate the drift [12]. Nowadays, there are

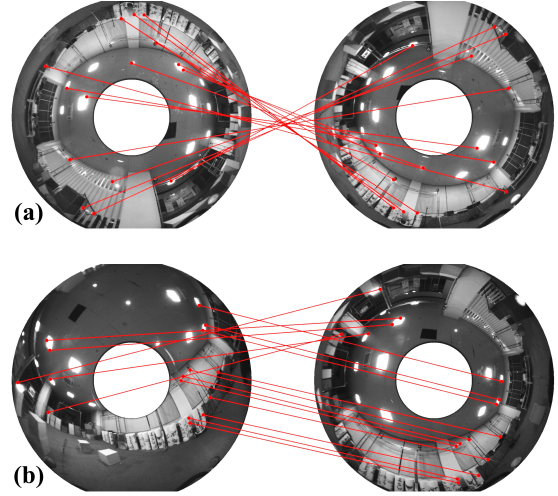


Fig. 1. Our loop images with large attitude differences (for illustration purposes, the illumination and contrast of the panoramas are improved) in scenarios (a) large yaw angle difference and (b) large tilt angle difference.

existing VIO and VO frameworks with a loop closure module [13]–[15]. Unfortunately, they do not support large-FoV camera very well, due to the usage of $[u, v, 1]^T$ to represent the location of image feature points, which means that they discard the points on the negative half-plane that exceeds the 180° [16]–[18]. Meanwhile, contemporary VIO and VO frameworks [1], [17], [19] that support large-FoV cameras, lack a corresponding loop closure module. They focus on the neighboring-frame feature point matching, but neglect to exploit the attitude information, which are very important for robust feature descriptor extraction, especially, when working with large-FoV cameras that can provide more overlapping content for loop-closure frame matching and strengthen the attitude-invariance of feature descriptors.

However, while the panoramic FoV is seemingly advantageous for loop closure, the benefits cannot easily be materialized under significant attitude differences, where loop-closure frames can hardly be matched by existing methods [13], [14]. In our recently proposed Large-FoV VIO (LF-VIO) system [19], for incorporating abundant cues on the negative plane of the panoramic lens, image features are represented as a three-dimensional vector with a unit length, which helps to greatly improve the estimation accuracy. Nevertheless, it still fails to fully unleash the potential of the ultra-wide FoV without a proper loop closure design.

To tackle this challenge, we propose *LF-VIO-Loop*, a loop closure framework that supports the negative plane with large-FoV cameras. There are negative half-plane cameras [6], and since the horizontal FoV is 360°, their images can be rotated around the center like fisheye-, panoramic

*This was supported in part by the National Natural Science Foundation of China (Grant No. 12174341), in part by the Federal Ministry of Labor and Social Affairs (BMAS) through the AccessibleMaps project under Grant 01KM151112, in part by the University of Excellence through the “KIT Future Fields” project, in part by Hangzhou SurImage Technology Co. Ltd., and in part by Hangzhou HuanJun Technology Co. Ltd. (Corresponding author: Kaiwei Wang and Kailun Yang.)

¹State Key Laboratory of Modern Optical Instrumentation, Zhejiang University, China

²Institute for Anthropomatics and Robotics, Karlsruhe Institute of Technology, Germany

³State Key Laboratory of Industrial Control Technology, Zhejiang University, China

⁴Huzhou Institute of Zhejiang University, Zhejiang University, China.
Email: {wangze0527, peng_li, fgaoaa, wangkaiwei}@zju.edu.cn, kailun.yang@kit.edu

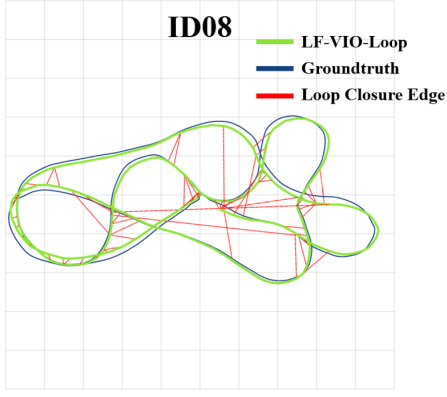


Fig. 2. LF-VIO-Loop’s loop closure effect in ID08 on the PALVIO dataset [19]. The side length of each gray square is 1m.

annular-, and catadioptric cameras. Since the attitude information of the VIO system can be obtained in the loop closure thread, we propose to make full use of this information to improve the efficiency and accuracy of the loop closure. In this way, the frames can be robustly matched, despite the large difference in tilt- and yaw angle, as illustrated in Fig. 1, thus, boosting the accuracy of the loop closure.

When we seize the unit vector used in LF-VIO [19] to represent the feature points, the traditional Random Sample Consensus (RANSAC) method [20] does not reject the outlier well, which will lead to a large error in loop closure. Therefore, we propose a loop closure framework with an RANSAC method to enhance the VIO accuracy. Our loop closure thread consists of four main processes: descriptor extraction, DBow query, the improved RANSAC method, and pose graph optimization. We use the attitude information to make the descriptor matching more robust and improve the RANSAC method to enhance the overall system accuracy.

We conduct a comprehensive variety of experiments on the PALVIO dataset [19] including descriptor matching experiment and loop closure precision experiment. Our approach significantly elevates the performance of the previous state-of-the-art large-FoV VIO framework LF-VIO [19] on all sequences. Our descriptor with attitude guidance outperforms the BRIEF descriptor [21] and even deep learning based methods SuperPoint [22] and GMS [23]. LF-VIO-Loop has higher accuracy overall compared to VINS-Loop [13] and SVO2.0-Loop [14]. As shown in Fig. 2, LF-VIO-Loop can successfully close the loop even at very long distances.

In summary, we deliver the following contributions:

- We propose *LF-VIO-Loop*, a loop closure framework for cameras with a large field of view.
- We propose a method to assist the descriptor extraction with VIO attitude information in loop closure detection.
- We introduce a novel RANSAC method to reject outlier points for solving the pose transformation between loop-closure frames and keyframes robustly.
- *LF-VIO-Loop* has attained significantly better accuracy compared to that without loop closure on *ID01~ID10* of PALVIO, a panoramic annular camera dataset.

II. RELATED WORK

In this section, a brief review of representative works is presented on visual inertial odometry with loop closure and panoramic SLAM frameworks.

A. Visual Inertial Odometry with Loop Closure

The VIO system obtains its own position, attitude, velocity, and other state estimation quantities through vision sensors and Inertial Measurement Units (IMU) [13]. Due to the lack of absolute position such as the Global Navigation Satellite System (GNSS) and heading angle observation such as the magnetometer, its position and yaw angle will drift over time. Because of the presence of accelerometer measurements, the pitch and roll angles do not diverge and the drift is small and the yaw angle does not diverge if the magnetometer is present. Therefore, loop closure correction of position and yaw angle to obtain the offset is crucial. VINS [13] proposed a robust and universal monocular vision inertial state estimator. SVO2.0 [14], the Semi-direct Visual-inertial Odometry, has recently been released for different camera models with loop closure. ORB-SLAM3 [15] introduced an accurate open-source library for vision, visual inertial, and multi-map SLAM. These open-source VIO frameworks have loop closure modules, but the unique characteristics of large-FoV cameras are not considered. As pointed out in LF-VIO [19], they characterize feature points using a representation of $[u, v, 1]^T$ and do not well support scenarios with a negative imaging plane. In this work, we enhance LF-VIO and present a loop closure framework specifically designed for wide-FoV cameras by unlocking their potential in matching loop-closure frames with attitude guidance.

B. Panoramic SLAM Frameworks

Panoramic cameras have better robustness to environments with weak textures due to their wider sensing range and captured richer features [6], [8], [24]. Therefore. There are many VO and VIO frameworks based on panoramic cameras.

Sumikura *et al.* [25] proposed OpenVSLAM, which is a VO framework supporting panoramic cameras. Wang *et al.* [26] put forward CubemapSLAM, a piecewise-pinhole monocular fisheye SLAM system. Chen *et al.* [1], [2] tackled VO with a panoramic annular camera. More recently, Wang *et al.* [17] proposed PAL-SLAM, which supports panoramic annular cameras. Huang *et al.* [18] proposed 360VO, a novel direct visual odometry algorithm. However, the above and many current VO and VIO frameworks do not have modules for loop closure [27]–[29], whereas some panoramic SLAM frameworks [26], [30] convert panoramic images into multiple pinhole images, which can be processed in parallel via a multi-thread program, but sacrifice the 360° consistency of the panoramic images. In this work, loop closure is directly performed on panoramas to fully materialize the benefits of 360° content.

III. LF-VIO-LOOP: PROPOSED FRAMEWORK

In this work, we propose a loop closure framework for large-FoV cameras, established upon our previous LF-VIO [19], a visual-inertial-odometry system that can make

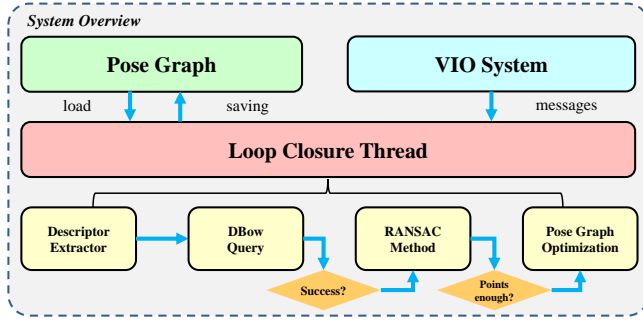


Fig. 3. Flow of our VIO system with loop closure.

use of feature points appearing on the negative imaging plane. The threads of our loop closure are independent of the our VIO system [19], which need to provide the position of its extracted feature points in the image, the three-dimensional coordinates of the feature points in the camera coordinate system, and the rotation matrix R_c^w and translation vectors T_c^w of the VIO system at the current t . The flow of our VIO system with loop closure is shown in the Fig. 3.

When receiving information from the VIO system, we first transform the image using the pose information, and then extract the descriptors of the feature points. DBow [31] is utilized to transform them to a Bag-of-Words (BoW) vector. We use the BoW database to check if the current frames are similar to the historical frames. In loop closure detection, it may happen that the descriptors between two frames are close, but many feature points are mis-matched. This situation is less likely to occur with pinhole cameras with a small FoV. However, it is more likely to occur with large-FoV cameras, where a wrong match can have a significant negative impact on the pose graph optimization.

Therefore, it is very important to ensure the accuracy and precision of loop closure with large-FoV cameras by effectively eliminating the outlier points. Then, in Sec. III-A, we present our improved loop closure detection method with attitude guidance. In Sec. III-B, we detail our designed epipolar constraint RANSAC method. In Sec. III-C and Sec. III-D, we describe the adapted EPnP RANSAC method for incorporating negative-imaging-plane features points and our pose graph optimization process.

A. Improved Loop Closure Detection

In matching loop-closure frames, feature matching methods are involved and they rely on descriptors, such as BRIEF [21], SuperPoint [22], and GMS [23]. For large-FoV cameras with a negative imaging plane, when the attitude difference is too large, the descriptor information difference is significant. Therefore, direct matching of the original image is often not very effective, which will be unfolded in Sec. IV. Compared with pinhole cameras, cameras with a large FoV have a higher probability of matching in the loop closure (see a comparison of the FoV of a conventional pinhole camera and a panoramic annular camera in Fig. 4). Yet, at the same time, the loop closure detection rate is not high, due to the large difference between the pose of the loop-closure frames and the keyframes. Therefore, we propose

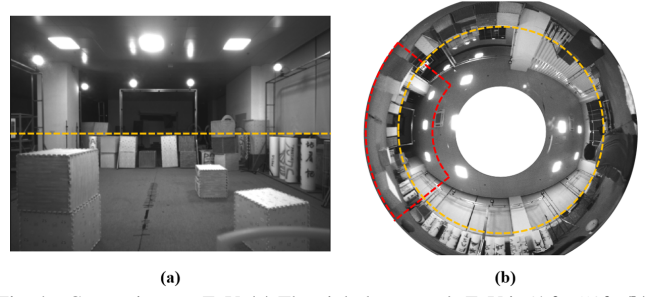


Fig. 4. Comparison on FoV. (a) The pinhole camera's FoV is $87^\circ \times 58^\circ$. (b) The panoramic camera's FoV is $360^\circ \times (40^\circ \sim 120^\circ)$. The orange dashed line is the horizontal line of the stationary position. The red dashed line denotes the area (a) in the FoV of (b).

to use the pose information provided by VIO to remap the images and then extract the descriptors, which can greatly improve the success rate of descriptor matching. For each point in the original image denoted as $[u, v]^T$, the coordinates of the transformed point are $[u_1, v_1]^T$, and the transformation relationship is depicted in Eq. (1).

$$\begin{bmatrix} u_1 \\ v_1 \end{bmatrix} = \pi_s \left(R_b^w R_c^b \pi_s^{-1} \left(\begin{bmatrix} u \\ v \end{bmatrix} \right) \right), \quad (1)$$

where R_b^w is the rotation matrix from the body coordinate system to the world coordinate system, R_c^b is the rotation matrix from the camera coordinate system to the body coordinate system, and π_s means the mapping relationship from the unit 3D coordinate point to the pixel point. For cameras with a negative plane, π_s is defined in Eq. (2).

$$\begin{bmatrix} \alpha \\ \beta \\ \gamma \end{bmatrix} = \pi_s^{-1} \left(\begin{bmatrix} u \\ v \end{bmatrix} \right), \alpha^2 + \beta^2 + \gamma^2 = 1. \quad (2)$$

B. Epipolar Constraint RANSAC

Since features have more outlier points in loop closure matching than in a conventional VIO system (*i.e.*, in the neighboring-frame matching), if the feature points are incorrectly matched, it will seriously affect the pose solving of loop-closure frames and keyframes, thus affecting the accuracy of loop-closure optimization, so the RANSAC method is crucial in loop-closure threads. In loop closure, the pair of two points x_1, x_2 , is obtained via descriptors matching as shown in Fig. 5, and they are used for solving the pose via Eq. (3)(4).

$$x_2^T ([T]^\wedge R) x_1 = 0, \quad (3)$$

$$x_1 = \begin{bmatrix} \alpha_1 \\ \beta_1 \\ \gamma_1 \end{bmatrix}, x_2 = \begin{bmatrix} \alpha_2 \\ \beta_2 \\ \gamma_2 \end{bmatrix}, \quad (4)$$

where the notation $[T]^\wedge$ denotes the skew-symmetric cross product matrix of $T \in \mathbb{R}^3$. Given x_1, T , and R , if x_2 satisfies the epipolar constraint, $-x_2$ must also satisfy the constraint. This does not happen with cameras that have only a positive imaging half-plane. For large-FoV cameras with a negative plane, the number of outlier points, which can be rejected using only the epipolar constraint, is relatively small. Therefore, we propose a novel method to avoid this situation. Points on the red epipolar line, as depicted in Fig. 5, can be

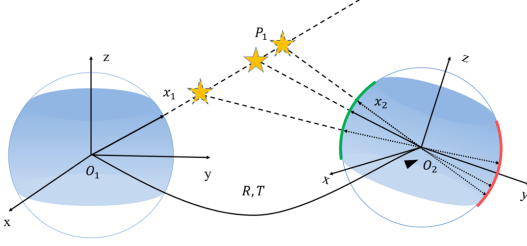


Fig. 5. Epipolar constraint. The orange pentagrams indicate landmarks, and each pentagram corresponds to the two vectors on the right, where vector vertices on the green line are retained and on the red line are removed.

effectively eliminated in our method. Our epipolar constraint RANSAC method has the following four steps:

- 1) Each time 8 points are selected from all pairs of points, then the essence matrix is calculated and the score of each point is calculated. We eliminate outlier points that do not satisfy the epipolar constraint.
- 2) The decomposition of the highest scoring essential matrix yields four groups R_m and T_m ($m=1, 2, 3, 4$).
- 3) The dot product between Q_i and $R_m P_i$ should be greater than the threshold, and again we use the scoring mechanism to eliminate the remaining outlier points.

This process is summarized via pseudocode in **Algorithm 1**.

C. EPnP RANSAC for Unit Vector Feature Points

Since we use the unit vectors as introduced in LF-VIO [19] to characterize the feature points, EPnP [32] needs to consider the negative imaging plane case when checking the inlier points. We make sure that, the angle between the map point and the feature point in the camera coordinate system is less than the threshold value, to filter out inlier points. The pseudocode of this process is summarized in **Algorithm 2**.

D. Pose Graph Optimization

Pose graph optimization plays a role in error correction in loop closure thread. To optimize each node in the pose graph, we minimize the following cost function to optimize the whole graph of loop closure edges and sequential edges via Eq. (5)(6).

$$\min_{p, \psi} \left\{ \sum_{(i,j) \in \mathcal{L}} \|r_{i,j}\|^2 + \sum_{(i,j) \in \mathcal{S}} \|r_{i,j}\|^2 \right\}, \quad (5)$$

$$r_{i,j} (p_i^w, \psi_i, p_j^w, \psi_j) = \begin{bmatrix} R(\hat{\phi}_i, \hat{\theta}_i, \psi_i)^{-1} (p_j^w - p_i^w) - \hat{p}_{ij}^i \\ \psi_j - \psi_i - \hat{\psi}_{ij} \end{bmatrix}, \quad (6)$$

where $\hat{\phi}_i$ and $\hat{\theta}_i$ are the fixed estimates of roll and pitch angles, because for a VIO system the roll and pitch angles do not diverge due to the accelerometer, and \mathcal{S} and \mathcal{L} are the sets of all sequential edge and loop closure edge.

Pose graph saving and loading allows us to use priori maps for loop closure. We only save descriptors of every keyframes and the i th keyframe's state is depicted in Eq. (7).

$$\left[i, \hat{p}_i^w, \hat{q}_i^w, v, \hat{p}_{iv}^i, \hat{\psi}_{iv}, D(\alpha, \beta, \gamma, des) \right], \quad (7)$$

Algorithm 1: Epipolar Constraint RANSAC Method

Input: pairs of feature points sets $\{P\}$, $\{Q\}$, iteration number K

Output: points status sets $\{S\}$ (1: inlier point, 0: outlier point), the flag that the algorithm has a solution $flag$ (1: success, 0: failure)

```

begin
  Initialization:  $best\_E, best\_score \leftarrow 0$ 
   $match\_num \leftarrow \text{elementNumber}(\{P\});$ 
  if  $match\_num < 8$  then
     $flag \leftarrow 0;$ 
    return  $flag;$ 
  for  $i \leftarrow 1$  to  $K$  do
    Randomly choose 8 pairs of points  $\{P_j\}, \{Q_j\};$ 
     $E \leftarrow \text{ComputeEssentialMatrix}(\{P_j\}, \{Q_j\});$ 
     $score, \{S_{tmp}\} \leftarrow \text{CheckInliers}(E, \{P\}, \{Q\});$ 
    if  $score > best\_score$  then
       $best\_score \leftarrow score;$ 
       $best\_E \leftarrow E;$ 
       $\{S_{best}\} \leftarrow \{S_{tmp}\};$ 
   $R_m, T_m \leftarrow \text{DecomposeEssentialMat}(best\_E);$ 
   $\{C_i\} \leftarrow \text{triangulatePoints}(R_m, T_m, \{P_i\}, \{Q_i\});$ 
  for  $i \leftarrow 1$  to  $match\_num$  do
    for  $j \leftarrow 1$  to  $m$  do
       $PdotC = P_i^T C_i / \|C_i\|_2;$ 
       $tmpC = R_j C_i + T_j;$ 
       $QdotC = Q_i^T tmpC / \|tmpC\|_2;$ 
      if  $PdotC < th$  and  $QdotC < th$  and
          $Q_i^T R_j P_i < th2$  then
         $good_j \leftarrow good_j + 1;$ 
         $S_j[i] \leftarrow 0;$ 
  if  $good_a \geq good_b$  then
    for  $i \leftarrow 1$  to  $match\_num$  do
      if  $S_a[i] == 0$  then
         $S_{best}[i] \leftarrow 0$ 
   $flag \leftarrow 1, \{S\} \leftarrow \{S_{best}\};$ 
  return  $flag, \{S\};$ 

```

where i , \hat{p}_i^w , and \hat{q}_i^w are the frame index, position, and orientation. v , \hat{p}_{iv}^i , and $\hat{\psi}_{iv}$ are the loop closure index, relative position, and yaw. $D(\alpha, \beta, \gamma, des)$ is the feature set containing the unit 3-D location and its descriptor after our attitude-guided transformation.

IV. EXPERIMENTS

A. Experiment Setup

In this section, a comprehensive variety of comparison experiments is conducted on the PALVIO dataset [19], an open-source large-FoV dataset captured by using a Panoramic Annular Lens (PAL) camera and an IMU sensor. This dataset has 10 sequences: ID01 to ID10, which are collected in a tight and complex space. Thus, it is very suitable for loop closure experiments. We only leverage the IMU sensor and the top PAL camera, whose FoV is $360^\circ \times (40^\circ \sim 120^\circ)$ with many information appearing on the negative imaging plane, i.e., $360^\circ \times (90^\circ \sim 120^\circ)$. The groundtruth pose and location are acquired via a motion capture device.

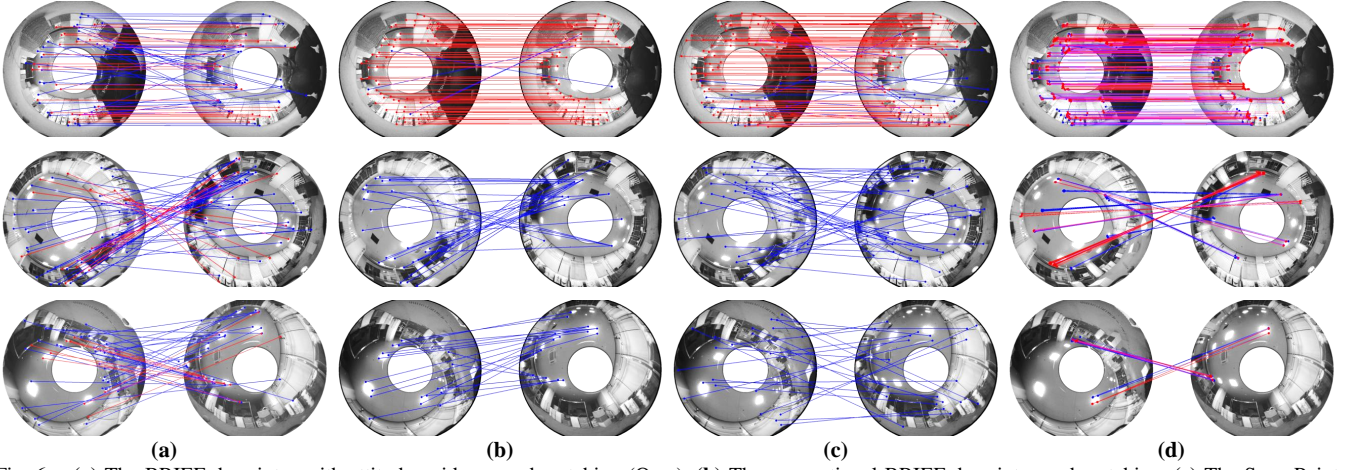


Fig. 6. (a) The BRIEF descriptor with attitude guidance and matching (Ours). (b) The conventional BRIEF descriptor and matching. (c) The SuperPoint descriptor and matching [22]. (d) The GMS matching [23]. For illustration purposes, the illumination and contrast of the panoramic images are improved. The three rows indicate scenarios with small angle differences, large yaw angle differences, and large tilt angle differences, respectively. The entire blue and red points represent all the matched points, and the red points are the remaining points after applying our RANSAC method.

Algorithm 2: Our EPnP RANSAC Method

Input: pairs of feature points set and matched landmark Points $\{P\}$, $\{W\}$, iteration number K
Output: Rotation Matrix R , translation vector T , points status sets $\{S\}$, the flag that the algorithm has a solution $flag$

```

begin
  Initialization:  $best\_score \leftarrow 0$ 
   $match\_num \leftarrow \text{elementNumber}(\{P\})$ ;
  if  $match\_num < 4$  then
     $flag \leftarrow 0$ ;
    return  $flag$ ;
  for  $i \leftarrow 1$  to  $K$  do
    Randomly choose 4 pairs of points  $\{P_j\}$ ,  $\{W_j\}$ ;
     $R_{tmp}, T_{tmp} \leftarrow \text{ComputePoseByEpnP}(\{P_j\}, \{W_j\})$ ;
     $score, \{S_{tmp}\} \leftarrow \text{CheckInliers}(R_{tmp}, T_{tmp}, \{P\}, \{W\})$ ;
    if  $score > best\_score$  then
       $best\_score \leftarrow score$ ;
       $R \leftarrow R_{tmp}$ ;
       $T \leftarrow T_{tmp}$ ;
       $\{S_{best}\} \leftarrow \{S_{tmp}\}$ ;
   $flag \leftarrow 1, \{S\} \leftarrow \{S_{best}\}$ ;
  return  $R, T, flag, \{S\}$ ;

```

B. On the Effectiveness of Attitude-Guide Descriptors

To verify that the introduction of attitude-guided descriptors is more effective than the direct extraction of descriptors, we explore different settings including (a) transform the images with attitude guidance and extract BRIEF descriptors for matching using Hamming distance, (b) directly extract BRIEF descriptors [21] for matching, (c) directly extract SuperPoint descriptors [22] for matching, and (d) the GMS solution [23] in comparison experiments with small attitude angle differences, large yaw angle differences, and large tilt angle differences, as shown in the three rows in Fig. 6, respectively. To facilitate a fair comparison, our RANSAC is used to remove the outliers for the above methods. The original number of ORB points [15] in the GMS is 1000,

and the rest only uses 500 points.

As shown in the first row, when the difference between the attitude angles of the two images is very small, our method matches more error points compared with the other three methods, but all the outlier points can be removed by the RANSAC method. As shown in the second row, when the difference between the yaw angles of the two images is large, the conventional BRIEF and the learning-based SuperPoint basically do not match the correct points at all, and the performance of GMS and our method is close. As shown in the third row, when the yaw angles of the two panoramic images differ significantly, our algorithm has an obvious advantage over the other three algorithms, in which BRIEF and SuperPoint methods struggle to match correct points, and the GMS solution matches relatively more yet all close points, so the effect is rather unsatisfactory. Thus, our method is more effective than other algorithms under large attitude angle differences, despite that the learning-based GMS uses a bigger number of original points for matching. It is possible to perform loop closure even when the angle difference is very large, so that the success rate of loop-closure matching can be improved, promising for improving pose estimation accuracy with large-FoV panoramic cameras.

C. Comparison on the Public PALVIO Dataset

Since most of the data in the public PALVIO dataset are collected in indoor areas, these sequences are suitable for loop closure accuracy experiments. Our LF-VIO-Loop is an addition of loop closure threads to LF-VIO [19]. At the same time, we also compare with SVO2.0 [14] and VINS-Mono [13], both of which have loop closure threads for a fair comparison in Table I and Fig. 7. We utilize the Relative Pose Error in translation (RPET), Relative Pose Error in rotation (RPER), and Absolute Trajectory Error (ATE) [33] as the evaluation metrics of the overall system error. The above four methods all use the Scaramuzza *et al.*'s omnidirectional camera model [34] to keep a fair comparison.

Due to the characteristics of large-FoV panoramic cameras with a negative imaging plane, VINS and SVO2.0, relying

TABLE I
COMPARISON OF VIO METHODS ON THE PALVIO DATASET [19].

VIO-Method		Sequences									
		ID01	ID02	ID03	ID04	ID05	ID06	ID07	ID08	ID09	ID10
LF-VIO-Loop	RPEt (%)	2.861	2.576	2.367	1.379	1.858	2.386	1.647	2.346	1.591	3.525
	RPEr (degree/m)	0.307	0.362	0.208	0.178	0.235	0.386	0.224	0.192	0.140	0.558
	ATE (m)	0.229	0.143	0.130	0.129	0.143	0.083	0.138	0.135	0.113	0.180
LF-VIO [19]	RPEt (%)	3.556	2.709	2.542	1.495	2.016	2.814	2.775	2.983	2.146	4.493
	RPEr (degree/m)	0.328	0.599	0.292	0.227	0.328	0.397	0.315	0.202	0.322	0.567
	ATE (m)	0.341	0.153	0.269	0.166	0.200	0.093	0.237	0.236	0.222	0.292
SVO2.0-Loop [14]	RPEt (%)	6.531	6.995	2.710	1.928	2.354	3.409	3.718	2.811	2.012	14.147
	RPEr (degree/m)	0.401	0.378	0.235	0.165	0.296	0.320	0.187	0.291	0.230	0.608
	ATE (m)	0.761	0.380	0.366	0.174	0.148	0.124	0.428	0.236	0.292	1.122
VINS-Mono-Loop [13]	RPEt (%)	5.446	3.542	2.767	2.189	2.553	2.993	2.941	2.405	2.933	4.494
	RPEr (degree/m)	0.4577	0.605	0.285	0.249	0.278	0.445	0.339	0.452	0.457	0.567
	ATE (m)	0.870	0.214	0.310	0.217	0.263	0.104	0.299	0.194	0.378	0.557

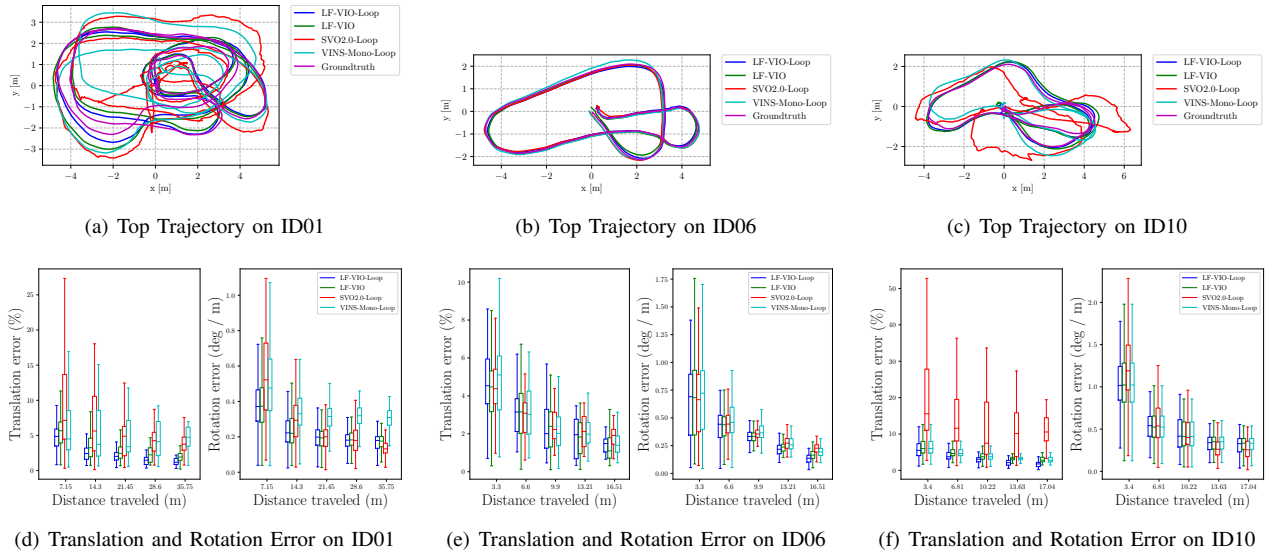


Fig. 7. Examples of top trajectories and error analyses on the PALVIO benchmark for different VIO systems.

on a representation of $[u, v, 1]^T$, can only make use of the positive half-plane image. Thus, even if similar images are detected, the useful feature point pairs are still rejected. For VINS-Mono-Loop, even its loop closure threads are enabled, it does not trigger the loop closure optimization with dissimilar images and insufficient feature points.

As shown in Table I, it can be seen that in all sequences (ID01 to ID10), LF-VIO-Loop has a highest precision in RPEt and ATE compared to the previous LF-VIO [19], SVO2.0 [14], and VINS-Mono-Loop [13]. Our approach significantly elevates the performance of the prior state-of-the-art large-FoV VIO framework LF-VIO. The effect of our loop closure in ID08 is visualized in Fig. 2, which demonstrates that our method can close the loop even at very long distances. Moreover, LF-VIO-Loop also has better precision scores in RPEt than LF-VIO and VINS-Mono-Loop in all sequences and SVO2.0 in most sequences. Following

LV-VIO [19], we present Top Trajectory, Translation, and Rotation Errors for sequences ID01, ID06, and ID10, as shown in Fig. 7. Evidently, our method is more accurate and more robust than other algorithms.

V. CONCLUSIONS

In this paper, we have proposed LF-VIO-Loop, an attitude-guided loop closure framework for large-FoV cameras. In the loop closure thread, we make use of the VIO system's attitude information to extract feature descriptors. Compared with the BRIEF descriptor, SuperPoint, and GMS, our method has better performance when the tilt angle or the yaw angle of the two loop-closure frames is very different. Our RANSAC method is more suitable for cameras with negative half-plane to reject outlier points. LF-VIO-Loop has a higher accuracy compared to VINS-Mono-Loop and SVO2.0-Loop on the public PALVIO dataset. In the future, we aim to use stereo panoramic- and LiDAR sensors in our SLAM system.

REFERENCES

- [1] H. Chen, K. Wang, W. Hu, K. Yang, R. Cheng, X. Huang, and J. Bai, "Palvo: visual odometry based on panoramic annular lens," *Optics Express*, vol. 27, no. 17, pp. 24 481–24 497, 2019.
- [2] H. Chen, W. Hu, K. Yang, J. Bai, and K. Wang, "Panoramic annular SLAM with loop closure and global optimization," *Applied Optics*, vol. 60, no. 21, pp. 6264–6274, 2021.
- [3] K. Yang, X. Hu, H. Chen, K. Xiang, K. Wang, and R. Stiefelhagen, "DS-PASS: Detail-sensitive panoramic annular semantic segmentation through SwaftNet for surrounding sensing," in *2020 IEEE Intelligent Vehicles Symposium (IV)*, 2020, pp. 457–464.
- [4] H. Chen, K. Yang, W. Hu, J. Bai, and K. Wang, "Semantic visual odometry based on panoramic annular imaging," *Acta Optica Sinica*, vol. 41, no. 22, p. 2215002, 2021.
- [5] W. Hu, K. Wang, H. Chen, R. Cheng, and K. Yang, "An indoor positioning framework based on panoramic visual odometry for visually impaired people," *Measurement Science and Technology*, vol. 31, no. 1, p. 014006, 2019.
- [6] S. Gao, K. Yang, H. Shi, K. Wang, and J. Bai, "Review on panoramic imaging and its applications in scene understanding," *arXiv preprint arXiv:2205.05570*, 2022.
- [7] K. Yang, X. Hu, L. M. Bergasa, E. Romera, and K. Wang, "PASS: Panoramic annular semantic segmentation," *IEEE Transactions on Intelligent Transportation Systems*, vol. 21, no. 10, pp. 4171–4185, 2020.
- [8] K. Yang, J. Zhang, S. Reiß, X. Hu, and R. Stiefelhagen, "Capturing omni-range context for omnidirectional segmentation," in *2021 IEEE/CVF Conference on Computer Vision and Pattern Recognition (CVPR)*, 2021, pp. 1376–1386.
- [9] H. Shi, Y. Zhou, K. Yang, Y. Ye, X. Yin, Z. Yin, S. Meng, and K. Wang, "PanoFlow: Learning optical flow for panoramic images," *arXiv preprint arXiv:2202.13388*, 2022.
- [10] F. Caballero, L. Merino, J. Ferruz, and A. Ollero, "Vision-based odometry and SLAM for medium and high altitude flying UAVs," *Journal of Intelligent and Robotic Systems*, vol. 54, no. 1, pp. 137–161, 2009.
- [11] M. Maimone, Y. Cheng, and L. Matthies, "Two years of visual odometry on the mars exploration rovers," *Journal of Field Robotics*, vol. 24, no. 3, pp. 169–186, 2007.
- [12] A. Angeli, D. Filliat, S. Doncieux, and J.-A. Meyer, "Fast and incremental method for loop-closure detection using bags of visual words," *IEEE Transactions on Robotics*, vol. 24, no. 5, pp. 1027–1037, 2008.
- [13] T. Qin, P. Li, and S. Shen, "VINS-Mono: A robust and versatile monocular visual-inertial state estimator," *IEEE Transactions on Robotics*, vol. 34, no. 4, pp. 1004–1020, 2018.
- [14] C. Forster, M. Pizzoli, and D. Scaramuzza, "SVO: Fast semi-direct monocular visual odometry," in *2014 IEEE international conference on robotics and automation (ICRA)*, 2014, pp. 15–22.
- [15] C. Campos, R. Elvira, J. J. G. Rodríguez, J. M. Montiel, and J. D. Tardós, "ORB-SLAM3: An accurate open-source library for visual, visual-inertial, and multimap SLAM," *IEEE Transactions on Robotics*, vol. 37, no. 6, pp. 1874–1890, 2021.
- [16] H. Seok and J. Lim, "ROVO: Robust omnidirectional visual odometry for wide-baseline wide-FOV camera systems," in *2019 International Conference on Robotics and Automation (ICRA)*, 2019, pp. 6344–6350.
- [17] D. Wang, J. Wang, Y. Tian, K. Hu, and M. Xu, "PAL-SLAM: a feature-based SLAM system for a panoramic annular lens," *Optics Express*, vol. 30, no. 2, pp. 1099–1113, 2022.
- [18] H. Huang and S.-K. Yeung, "360VO: Visual odometry using a single 360 camera," in *2022 International Conference on Robotics and Automation (ICRA)*, 2022, pp. 5594–5600.
- [19] Z. Wang, K. Yang, H. Shi, P. Li, F. Gao, and K. Wang, "LF-VIO: A visual-inertial-odometry framework for large field-of-view cameras with negative plane," in *2022 IEEE/RSJ International Conference on Intelligent Robots and Systems (IROS)*, 2022.
- [20] M. A. Fischler and R. C. Bolles, "Random sample consensus: a paradigm for model fitting with applications to image analysis and automated cartography," *Communications of the ACM*, vol. 24, no. 6, pp. 381–395, 1981.
- [21] M. Calonder, V. Lepetit, C. Strecha, and P. Fua, "BRIEF: Binary robust independent elementary features," in *European Conference on Computer Vision*, 2010, pp. 778–792.
- [22] D. DeTone, T. Malisiewicz, and A. Rabinovich, "SuperPoint: Self-supervised interest point detection and description," in *2018 IEEE/CVF Conference on Computer Vision and Pattern Recognition Workshops (CVPRW)*, 2018, pp. 337–33712.
- [23] J. Bian, W.-Y. Lin, Y. Matsushita, S.-K. Yeung, T.-D. Nguyen, and M.-M. Cheng, "GMS: Grid-based motion statistics for fast, ultra-robust feature correspondence," in *2017 IEEE Conference on Computer Vision and Pattern Recognition (CVPR)*, 2017, pp. 2828–2837.
- [24] A. Jaus, K. Yang, and R. Stiefelhagen, "Panoramic panoptic segmentation: Towards complete surrounding understanding via unsupervised contrastive learning," in *2021 IEEE Intelligent Vehicles Symposium (IV)*, 2021, pp. 1421–1427.
- [25] S. Sumikura, M. Shibuya, and K. Sakurada, "OpenVSLAM: A versatile visual SLAM framework," in *Proceedings of the 27th ACM International Conference on Multimedia*, 2019, pp. 2292–2295.
- [26] Y. Wang, S. Cai, S.-J. Li, Y. Liu, Y. Guo, T. Li, and M.-M. Cheng, "CubemapSLAM: A piecewise-pinhole monocular fisheye SLAM system," in *Asian Conference on Computer Vision*, 2018, pp. 34–49.
- [27] C. Won, H. Seok, Z. Cui, M. Pollefeys, and J. Lim, "OmniSLAM: Omnidirectional localization and dense mapping for wide-baseline multi-camera systems," in *2020 IEEE International Conference on Robotics and Automation (ICRA)*, 2020, pp. 559–566.
- [28] H. Matsuki, L. Von Stumberg, V. Usenko, J. Stückler, and D. Cremers, "Omnidirectional DSO: Direct sparse odometry with fisheye cameras," *IEEE Robotics and Automation Letters*, vol. 3, no. 4, pp. 3693–3700, 2018.
- [29] M. Ramezani, K. Khoshelham, and C. Fraser, "Pose estimation by omnidirectional visual-inertial odometry," *Robotics and Autonomous Systems*, vol. 105, pp. 26–37, 2018.
- [30] H. Xu, Y. Zhang, B. Zhou, L. Wang, X. Yao, G. Meng, and S. Shen, "Omni-Swarm: A decentralized omnidirectional visual-inertial-UWB state estimation system for aerial swarms," *IEEE Transactions on Robotics*, 2022.
- [31] D. Gálvez-López and J. D. Tardos, "Bags of binary words for fast place recognition in image sequences," *IEEE Transactions on Robotics*, vol. 28, no. 5, pp. 1188–1197, 2012.
- [32] V. Lepetit, F. Moreno-Noguer, and P. Fua, "EPnP: An accurate O(n) solution to the pnp problem," *International Journal of Computer Vision*, vol. 81, no. 2, pp. 155–166, 2009.
- [33] Z. Zhang and D. Scaramuzza, "A tutorial on quantitative trajectory evaluation for visual (-inertial) odometry," in *2018 IEEE/RSJ International Conference on Intelligent Robots and Systems (IROS)*, 2018, pp. 7244–7251.
- [34] D. Scaramuzza, A. Martinelli, and R. Siegwart, "A toolbox for easily calibrating omnidirectional cameras," in *2006 IEEE/RSJ International Conference on Intelligent Robots and Systems (IROS)*, 2006, pp. 5695–5701.